Scilight

Water Scarcity and Drought
https://www.sciltp.com/journals/wsd

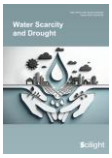

Article

Spatial Assessment of Dry-Spell Hazards in Spain: Toward an Operational Climate Service

Amar Halifa-Marín [1,2,*], S. Beguería [2,3], F. Reig [1,2], A. Royo-Aranda [1,2], M. Arretxea [4], M. Gil-Guallar [2,3], B. Latorre [2,3], A. El Kenawy [1,2], M. Franquesa [1,2], M. Adell-Michavila [1,2], A. Crespillo [1,2], D. Pérez-Pajuelo [1,2], F. Domínguez-Castro [1,2], J. M. Gutiérrez [5], C. Azorin-Molina [6], L. Gimeno [7,8,9], R. Nieto [7,8,9] and S. M. Vicente-Serrano [1,2]

[1] Instituto Pirenaico de Ecología, IPE-CSIC, Av. De Montañana 1005, 50059 Zaragoza, Spain
[2] Laboratorio de Climatologia y Servicios Climaticos (LCSC), CSIC—Universidad de Zaragoza, 50059 Zaragoza, Spain
[3] Estación Experimental de Aula Dei, EEAD-CSIC, 50059 Zaragoza, Spain
[4] Instituto de Geociencias (IGEO), Consejo Superior de Investigaciones Científicas—Universidad Complutense de Madrid (CSIC-UCM), 28040 Madrid, Spain
[5] Instituto de Fisica de Cantabria (IFCA), CSIC—Universidad de Cantabria, 39005 Santander, Spain
[6] Centro de Investigaciones Sobre Desertificación, Consejo Superior de Investigaciones Científicas (CIDE, CSIC-UV-Generalitat Valenciana), Climate, Atmosphere and Ocean Laboratory (Climatoc-Lab), Moncada, 46113 Valencia, Spain
[7] Environmental Physics Laboratory (EPhysLab), CIM-UVigo, Universidade de Vigo, 32004 Ourense, Spain
[8] Unidad Asociada CSIC-Universidad de Vigo: Grupo de Física de la Atmosfera y del Océano, 32004 Ourense, Spain
[9] Galicia Supercomputing Center (CESGA), 15705 Santiago de Compostela, Spain
* Correspondence: amar.halifa@ipe.csic.es

How To Cite: Halifa-Marín, A.; Beguería, S.; Reig, F.; et al. Spatial Assessment of Dry-Spell Hazards in Spain: Toward an Operational Climate Service. *Water Scarcity and Drought* **2025**, *1*(1), 4.

Received: 16 June 2025
Revised: 9 September 2025
Accepted: 25 September 2025
Published: 9 October 2025

Abstract: This study introduces the first high-resolution hazard probability maps for prolonged dry spells across Spain, marking a significant advancement toward a national climate service for drought extremes. Using long-term daily precipitation records from a dense network of meteorological stations and incorporating high-resolution topographic data, the methodology combines the fit of the dry spell series with a Generalized Pareto Distribution with universal kriging to spatially interpolate distribution parameters. The resulting maps provide robust and spatially continuous estimates of the likelihood and return periods of extreme dry spell durations, with strong validation against empirical station-based data. Our results reveal distinct spatial patterns in dry spell occurrence across Spain, with marked north-south gradients, highlighting the prevalence and severity of extended dry spells in southern and southeastern regions. Beyond the scientific contribution, the study delivers a fully operational, interactive online platform "https://rachas-secas.csic.es/ (accessed on 29 September 2025)" that allows end users to query localized drought hazards probabilities and return levels, supporting informed decision-making in sectors such as agriculture, water resource management, and ecosystem conservation. The flexible design of our employed methodological approach also offers potential for adaptation and replication in other regions globally, especially where dry spells pose significant socio-economic and environmental risks.

Keywords: dry spells; hazard probability maps; spatial interpolation; stationary models; climate services

1. Introduction

Droughts have significant environmental [1] and socioeconomic impacts [2]. Various approaches exist to assess the severity of drought events, often based on different variables and indices, including hydrological metrics

Copyright: © 2025 by the authors. This is an open access article under the terms and conditions of the Creative Commons Attribution (CC BY) license (https://creativecommons.org/licenses/by/4.0/).
Publisher's Note: Scilight stays neutral with regard to jurisdictional claims in published maps and institutional affiliations.

such as soil moisture [3,4] and streamflow [5,6]. However, a major limitation of this approach is the lack of available data globally, making it difficult to consistently assess drought hazard probabilities across space and time. A more widely used alternative is the use of atmospheric drought indices [7], which are based on meteorological variables—primarily precipitation and atmospheric evaporative demand [8,9]. These variables are generally available worldwide and allow for the assessment of long-term variability and spatial severity of droughts [10]. This method typically relies on standardized indices, which are normalized to have a mean of zero and a standard deviation of one, facilitating spatial and temporal comparisons across different variables.

Nevertheless, the use of standardized drought indices presents limitations, as they display identical units everywhere, limiting their ability to establish spatial differences in drought hazard probability. Therefore, further processing—such as identifying specific drought events and analyzing their duration and magnitude—is often required to derive meaningful spatial patterns [11]. These limitations can complicate interpretation from a climatological standpoint. To address this, approaches based on single variables recorded at high temporal frequency have been widely used in drought hazard assessment [12,13].

Precipitation data, in particular, have been frequently used, as prolonged periods of low rainfall are primary drivers of meteorological droughts [14]. Extended dry spells—defined as long sequences of days with scarce or no precipitation—can pose significant environmental impacts, including a substantial increase in the risk of forest decline and mortality [15], a reduction in crop yields in dryland areas [16], and a likely elevation in the probability of wildfires [17]. They also diminish water availability essential for hydropower, irrigation, urban, tourism, and industrial uses [18–20], triggering cascading effects that disrupt entire socioeconomic systems [21]. Because of these widespread impacts, dry-spell analysis has been extensively used to assess drought hazard probability [22–26] as regions with higher probabilities of long dry spells can be identified as being at greater risk of drought.

Recent global analysis has shown significant changes in the duration of extreme dry spells over the past 60 years [27]. Given the significant impacts of these long dry spells, it is essential to produce accurate spatial estimates of dry spell hazard probabilities. As drought is a significant factor in the occurrence of compound and cascading dry hazard phenomena, particularly in southern Europe and the Mediterranean, several recent studies have investigated the probability, frequency, and severity of dry-spell hazards in Southwest Europe and the Mediterranean [28–30]. In this regard, while digital maps for extreme precipitation events have become relatively common [31–34], examples of dry-spell hazard probability mapping remain scarce [22,35,36].

Spain is highly affected by drought events [37,38], which produce severe socioeconomic, agricultural, and ecological impacts [39–42]. For this reason, mapping dry-spell hazard probability at enhanced spatial scales is critical for informing territorial planning strategies that integrate precipitation-related hazards into environmental, economic, and social management. This makes the development of high-resolution maps depicting dry spell probabilities a priority in the country. In this study, we present, for the first time, spatial maps of dry spell duration quantiles across Spain and integrate this information into a climate service platform. This tool allows users to interactively explore return periods and quantiles of dry spell durations, providing a valuable resource for climate adaptation planning.

2. Data and Methods

2.1. Database

We used daily precipitation data from 2840 stations for 1961–2024 (Figure 1). These stations were selected from the full set of daily records provided by the Spanish Meteorological Agency (AEMET), which included raw data from nearly 11,000 stations. The dataset underwent rigorous quality control [43]. For stations with more than 35 years of original data, missing values were filled using a quantile matching approach based on data from neighbouring stations [44]. This procedure considered only stations with at least 15 years of overlapping data, which are located within a 50 km radius of the target station. Further details on this methodological procedure can be found in [45].

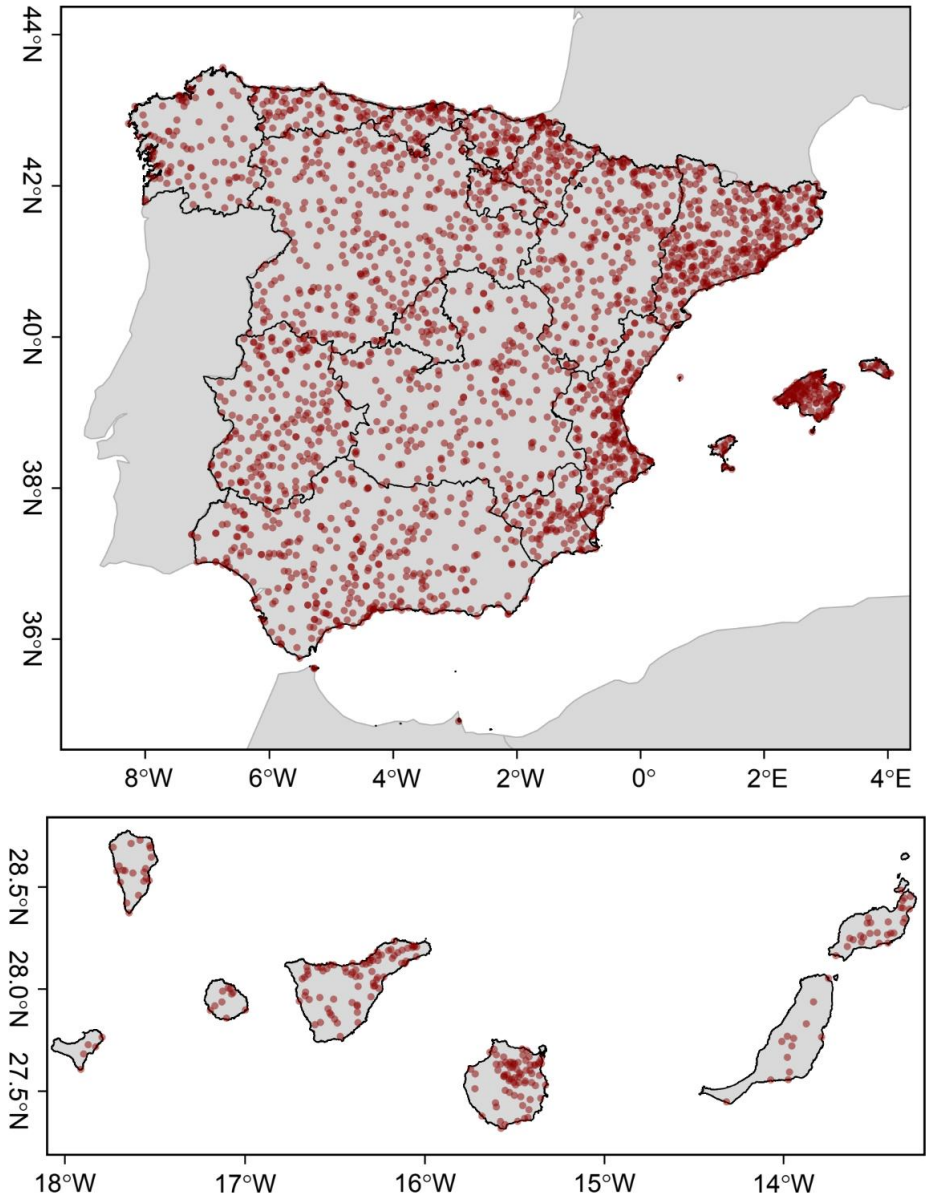

Figure 1. Spatial distribution of the precipitation stations used in this study: continental Spain and Balearic Islands (**upper**), and Canarias islands (**bottom**).

2.2. Methods

2.2.1. Selection of the Sample

This study builds on the methodological approach proposed by [46], albeit with several modifications. Our focus is on estimating the spatial hazard probability of dry spell duration, defined as consecutive days with zero millimetres of precipitation. We define days with <0.1 mm precipitation as dry, following AEMET's convention.

Various approaches have been developed to model the censored data corresponding to dry spell durations. For short dry spells, models such as Markov chains [24,25,47], the exponential distribution [48], the mixed geometric distribution [49], and the truncated negative binomial distribution [50,51], among others, have been employed. However, a key limitation of these models is their insensitivity to the upper tail of the distribution—precisely where the most impactful long dry spells occur. Although dry spell duration is inherently a censored (discrete) variable, the large range of values allows it to be reasonably approximated as continuous for the purpose of modelling extreme events.

Therefore, we applied extreme value theory (EVT) to estimate the probability of events exceeding a given threshold [52]. Here, we constructed partial duration (PD) series based on predefined thresholds, selecting only those values that exceed the threshold and defining the exceedances. Since the choice of threshold can influence the estimated dry spell quantiles [46], we evaluated several threshold selection methods. We used fixed

percentiles—namely the 90th, 92.5th, and 95th percentiles—as well as data-driven approaches such as the Hall estimator, based on extreme value theory to estimate the optimal tail fraction; mindist, which selects the threshold that minimizes the distance between empirical and theoretical distributions; PS (Pickands–Siegmund), which minimizes the bias–variance trade-off in tail estimation; and single and double bootstrap procedures (Gomes, Himp, dAMSE) for determining the optimal sample fraction [53].

2.2.2. Theoretical Framework

The series generated by exceedances over a threshold tend to converge to a Generalized Pareto (GP) distribution [54], a behavior that has been observed—even when censored—in dry-spell length series due to the wide variability of this variable [35,46,55]. The GP distribution is defined by an origin parameter (x_0), a shape parameter (κ), and a scale parameter (α), with the following cumulative distribution function:

$$P(\alpha,\kappa) = 1 - \left(1 - \kappa\frac{y}{\alpha}\right)^{\left(\frac{1}{\kappa}\right)}, (y_i = x_i - x_0).$$

In this study, GP distribution parameters were estimated using the probability-weighted moments method [56]. The exceedance probability of Y is often expressed through its return period t, which represents the expected time between two consecutive occurrences of the event. The return period is the inverse of the exceedance probability:

$$t_y = \frac{1}{\lambda[1-P(Y\leq y)]}$$

where λ is a frequency parameter representing the average number of exceedances per year in the dataset. The expected maximum value $E_y(t)$ over a period of t years is calculated as:

$$E_y(t) = x_0 + \frac{\alpha}{\kappa}\left[1 - \left(\frac{1}{\lambda t}\right)^{k}\right]$$

Uncertainty in these estimates strongly depends on the sample size—larger values are generally associated with higher uncertainty. For this reason, magnitude-frequency curves for different dry-spell durations are complemented by confidence interval estimations. The variances and covariance of α and κ are defined as:

$$Var(\alpha) = \frac{\alpha^2}{\lambda}\cdot\frac{7+18\kappa+11\kappa^2+2k^3}{(1+2\kappa)(3+2\kappa)}$$

$$Var(\kappa) = \frac{1}{\lambda}\cdot\frac{(1+\kappa)(2+\kappa)^2(1+\kappa+2\kappa^2)}{(1+2\kappa)(3+2\kappa)}$$

$$Cov(\alpha,\kappa) = \frac{\alpha}{\lambda}\cdot\frac{(2+\kappa)+(2+6\kappa+7\kappa^2+2\kappa^3)}{(1+2\kappa)(3+2\kappa)}$$

For a return period t and total time span A, the required partial derivatives are:

$$a_i = \frac{1}{k}\left(1 - \left(\frac{\lambda}{A}t\right)^{-\kappa}\right)$$

$$a_2 = \left(\frac{-\alpha}{\kappa^2}\right)\left(1 - \left(\frac{\lambda}{A}t\right)^{-\kappa}\right) + \left(\frac{\alpha}{\kappa}\right)\left(\frac{\lambda}{A}t\right)^{-\kappa} log\left(\frac{\lambda}{A}t\right)$$

The standard error S_T of the return period estimate is:

$$S_T = \sqrt{a_1^2 Var(\alpha) + a_2^2 Var(\kappa) + 2a_1a_2\cdot Cov(\alpha,\kappa)}$$

2.2.3. Spatial Mapping

Dry-spell quantiles can be estimated at individual meteorological stations and directly interpolated, as done in previous studies for both dry-spell [46] and extreme precipitation quantiles [57,58]. However, several studies have shown that interpolating distribution parameters outperforms direct quantile interpolation [59,60]. This approach also offers flexibility for user-defined, spatially distributed quantile calculations. For this reason, we interpolated the GP distribution parameters to improve estimation in regions lacking direct observations, following similar strategies previously applied to extreme precipitation mapping at a 2.5 km resolution [34,61].

To interpolate the parameters x_0, α, κ and λ, we applied a universal kriging algorithm [62], using geographic latitude, longitude, and elevation as auxiliary variables. Two zones were defined: (i) the Spanish mainland and Balearic Islands; and (ii) the Canary Islands. Up to 100 neighbouring observatories were used, with elevation and distance to the sea included as covariates. For semivariogram fitting, when the range was below 20 km or the sill was zero, a spherical model with a nugget effect was imposed. Interpolated layers were validated via a jack-knife

resampling procedure: parameters at individual stations were withheld, interpolated from remaining stations, and the difference between predicted and observed values was computed.

We applied different metrics for the validation procedure, including the mean absolute error (MAE), the Mean Error (ME), the Relative Standard Deviation (rSD), the Pearson correlation coefficient (r), the Kling-Gupta Efficiency (KGE), and the D agreement Index [63]. A more comprehensive and robust evaluation of model performance is facilitated by the use of a variety of validation metrics.

3. Results

3.1. On-Site Estimation and Validation

The method used to define the precipitation threshold for exceedance series generation yielded consistent values across the network (Figure 2). Some alternative approaches (e.g., gomes, Himp) produce high variability and elevated thresholds, which significantly reduced the sample size for probabilistic modeling. Using the 90th percentile of dry-spell duration yielded similar thresholds to those from other quantitative approaches (e.g., hall, mindist), with minimum differences compared to higher percentiles (92.5th, 95th). Thus, it is a suitable and conservative choice for Spain, maximizing sample size without including non-extreme events.

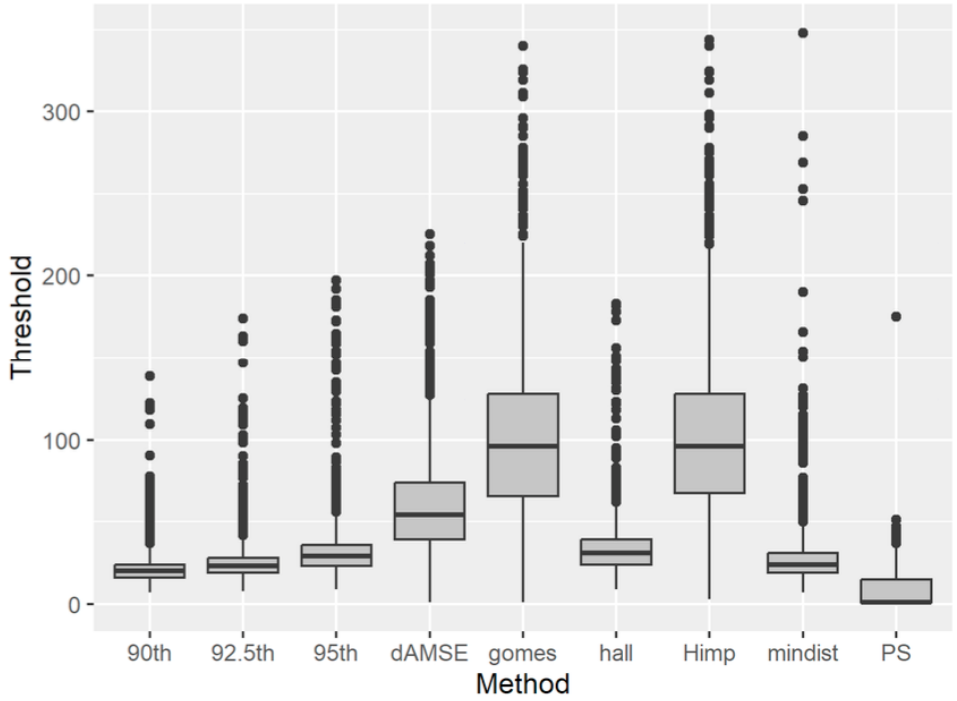

Figure 2. Comparison of the criteria used to define the threshold for constructing the peak-over-threshold series for extreme dry spells. The central line within each box represents the median, while the lower and upper edges of the box correspond to the first (Q1) and third (Q3) quartiles, respectively. The whiskers extend to the most extreme data points within 1.5 times the interquartile range (IQR) from the quartiles. Points beyond the whiskers indicate outliers. Threshold selection methods shown on the X-axis include: fixed percentiles (90th, 92.5th, 95th); dAMSE (double bootstrap minimizing asymptotic mean squared error); Gomes (bootstrap-based stability method); Hall estimator; Himp (single bootstrap procedure to select the optimal tail sample fraction by minimizing an AMSE-based criterion, improving on Hall's approach), mindist (minimum distance), PS (Pickands–Siegmund).

Figure 3 illustrates the strong fit between observed (empirical) and modeled cumulative distribution functions (CDF) for dry-spell durations at four representative meteorological stations using the GP distribution, demonstrating the performance of our threshold selection and the GP distribution's suitability. Figure 4 confirms this finding across all 2840 stations, showing high agreement based on R^2, the agreement index (d), and KGE. While the fit between empirical and modelled CDFs is consistently strong across the network (Figure 4), a few stations showed lower performance. These discrepancies likely reflect local climatic variability, complex topography, and shorter or fragmented records, which increase uncertainty in parameter estimation.

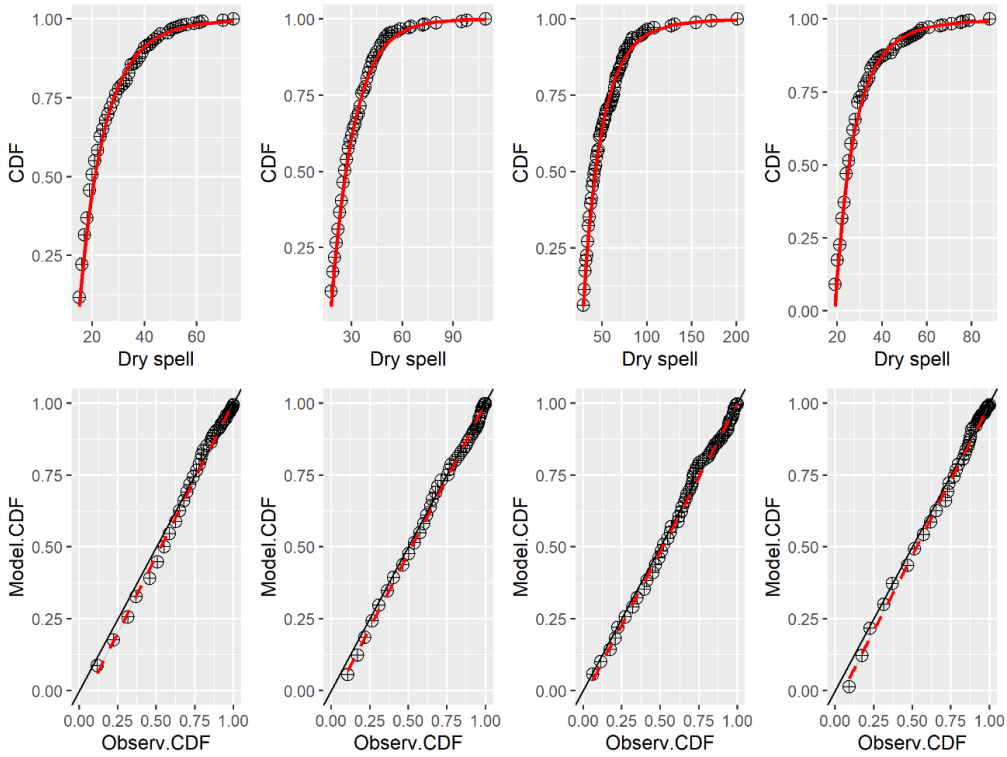

Figure 3. Top: Relationship between the observed duration of the dry-spells and the modelled CDF by means of the GP distribution. Bottom: Observed empirical CDF and GP distribution modelled CDF for the dry spell duration in four meteorological stations (Zaragoza, Madrid, Valencia and Sevilla).

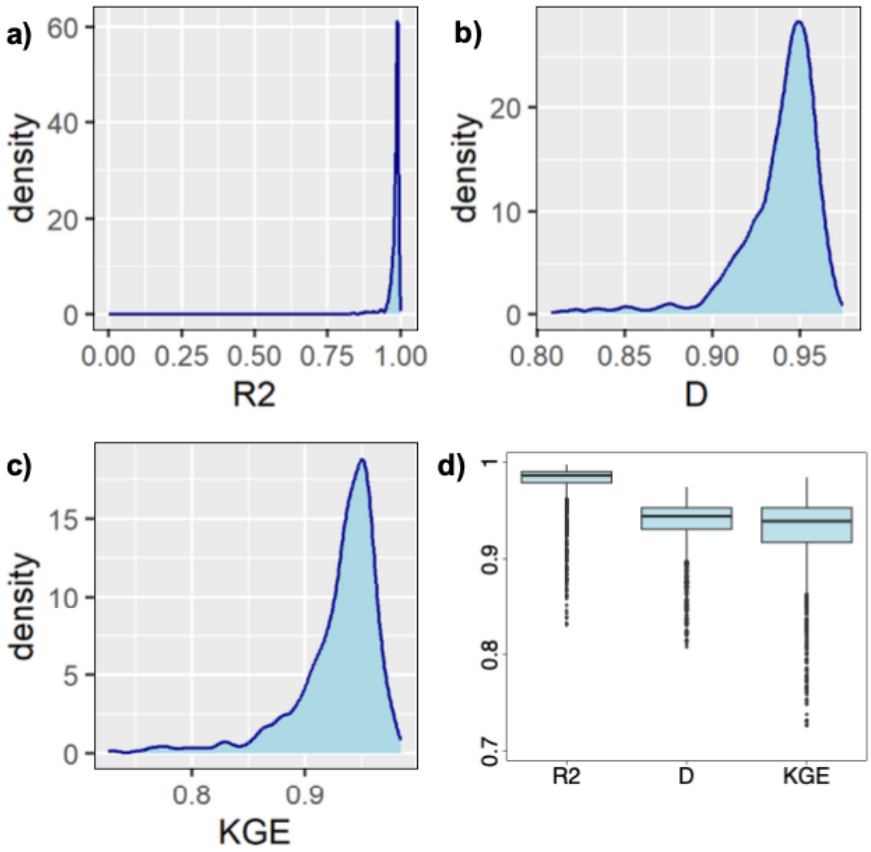

Figure 4. Validation of the goodness of fit between observed and modelled CDF for dry spell duration using the methodology of this study in the whole set of meteorological stations. Panels (**a**–**c**) represent the results for R2, D, and KGE analysis, and Panel (**d**) shows the boxplot for those metrics, identifying the median, interquartile range (with lines) and outliers (points) with values above the 90th percentile and below the 10th percentile.

3.2. Parameter Mapping

Spatial interpolation of GP distribution parameters reveals strong geographic coherence (Figure 5). In mainland Spain and the Balearic Islands, the α parameter showed a north-south gradient, with higher values in the south and modulation by topography. In the Canary Islands, despite their smaller area, α also exhibited clear spatial gradients related to elevation and west-east climatic differences.

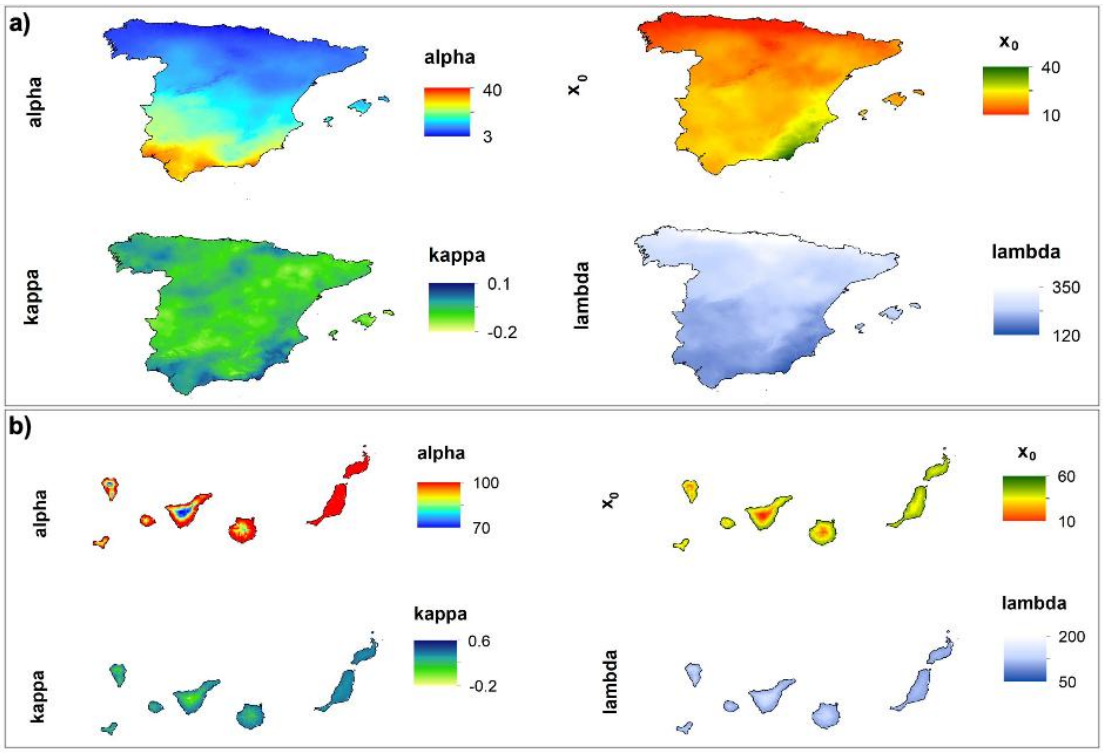

Figure 5. Spatial distribution of the alpha, kappa, x_0 and lambda corresponding to the maximum precipitation and total precipitation during the extreme precipitation events and the dry spell duration in the Iberian Peninsula and the Balearic Islands (**a**) and in the Canary Islands (**b**).

The origin parameter x_0 showed a similar pattern to α but with key differences—such as higher values in southeastern Spain. Topography also influences the spatial patterns, particularly in mountainous northern regions. The frequency parameter λ followed a north-south gradient, with maximum values in the north and minimum in the southeast. The shape parameter κ displayed greater spatial variability but showed identifiable patterns, with lower values in the southwestern and southeastern mainland and the western and southern Canary Islands.

Table 1 presents validation statistics from the jackknife procedure for each parameter. Agreement was found between observed and predicted values, especially for α, x_0 and λ, with rSD, KGE, and D values exceeding 0.9 in mainland Spain and the Balearic Islands. These statistics are slightly lower in the Canary Islands, reflecting greater climatic and topographic heterogeneity, but still indicate robust performance (e.g., $D > 0.8$). Notably, even κ showed reasonable agreement in the Canaries, supported by high rSD and D values.

Additional validation comes from Figures 6 and 7, which illustrate the distribution of observed versus interpolated GP parameters using violin plots. The similarity in the shape and central tendency of these distributions indicates that the interpolation process preserves the statistical characteristics of the original data, with no systematic bias for most parameters. This visual confirmation complements the cross-validation metrics in Table 1, reinforcing the reliability of the spatial interpolation approach. Although the validation metrics for the shape parameter κ were lower than those for the other parameters (Table 1), this behavior is expected given the higher sensitivity of κ to sample variability and the scarcity of extreme events. Despite this, κ exhibited a coherent spatial pattern and validation values clearly different from zero, particularly in the Canary Islands, where κ showed a well-defined spatial structure. These results indicate that, although κ tends to incorporate a more random component than other parameters, its spatial mapping provides valuable information compared to assuming a constant value.

Table 1. Cross-validation statistics for the different parameters: the mean absolute error (MAE), the Mean Error (ME), the Relative Standard Deviation (rSD), Pearson correlation coefficient (r), the Kling-Gupta Efficiency (KGE), and the D (Willmott agreement Index).

	Peninsular Spain and Balearic Islands					
	MAE	**ME**	**rSD**	**r**	**KGE**	**D**
alpha	1.72	0.02	0.95	0.94	0.92	0.97
kappa	0.05	0.00	0.61	0.49	0.36	0.65
x0	1.45	−0.03	0.94	0.93	0.90	0.96
length	11.69	0.19	0.96	0.95	0.94	0.98
	Canary Islands					
	MAE	ME	rSD	r	KGE	D
alpha	18.99	0.86	0.90	0.79	0.77	0.88
kappa	0.16	−0.01	0.85	0.76	0.70	0.86
x0	8.35	0.00	0.89	0.73	0.71	0.84
length	17.35	1.25	0.93	0.90	0.88	0.95

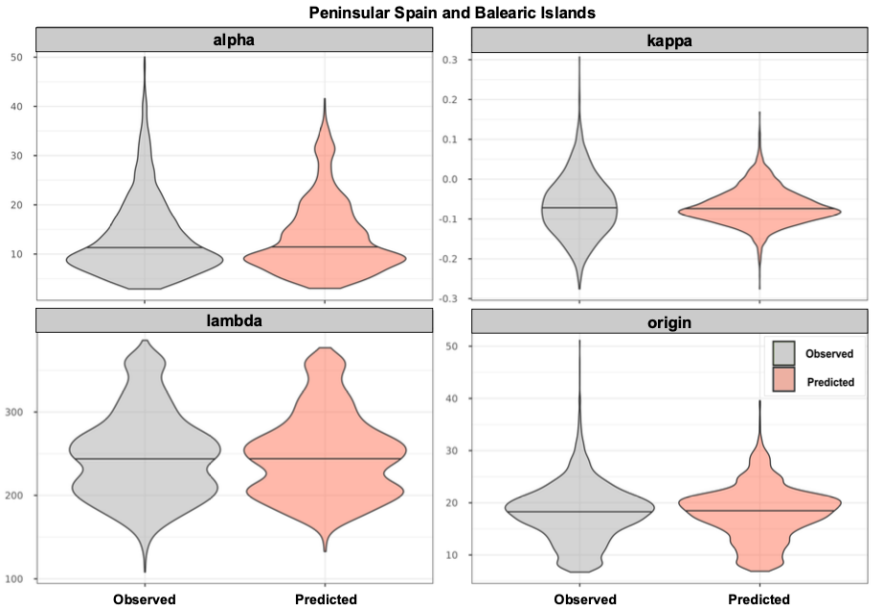

Figure 6. Violin plots comparing the observed and predicted parameters in the Peninsular Spain and Balearic Islands using the jack-knife cross-validation approach.

Figure 7. Violin plots comparing the observed and predicted parameters in the Canary Islands using the jack-knife cross-validation approach.

3.3. Long Dry-Spell Hazard Probabilities

Figure 8 shows the magnitude-frequency curves for dry-spell durations at selected stations, highlighting large spatial differences. Some locations may experience dry spells over 200 days once every 50 years, while others may not exceed 50 days over the same period.

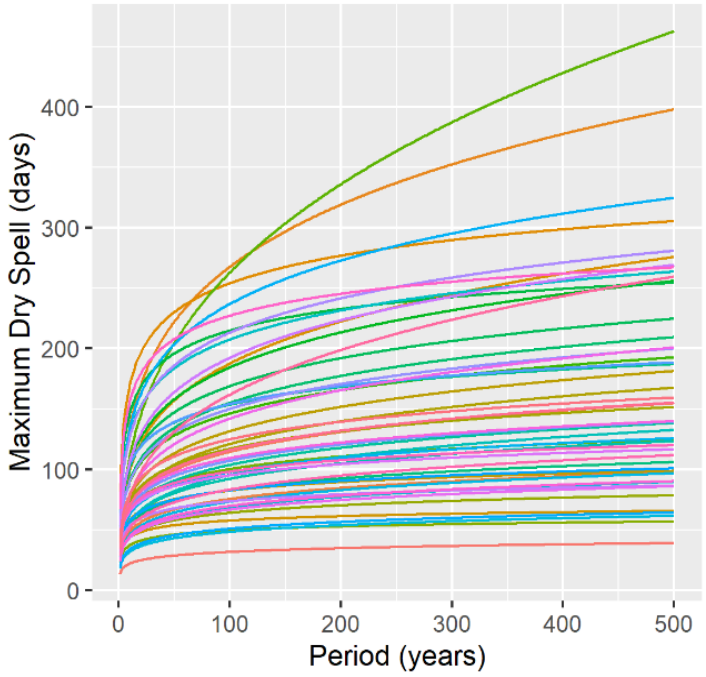

Figure 8. Examples of the quantile curves for 25 meteorological stations.

Quantile maps (Figure 9) clearly reflect spatial gradients. In mainland Spain and the Balearics, longer dry spells (e.g., >200 days in 100 years) are expected in the southwest. In the Canary Islands, western and eastern differences are evident—eastern islands, with their arid climate, may experience dry spells exceeding 500 days in 100 years. These patterns are consistent with return period maps for durations of 50, 100, and 150 days (Figure 10), which show much longer return periods in northern Spain and much shorter ones in the south.

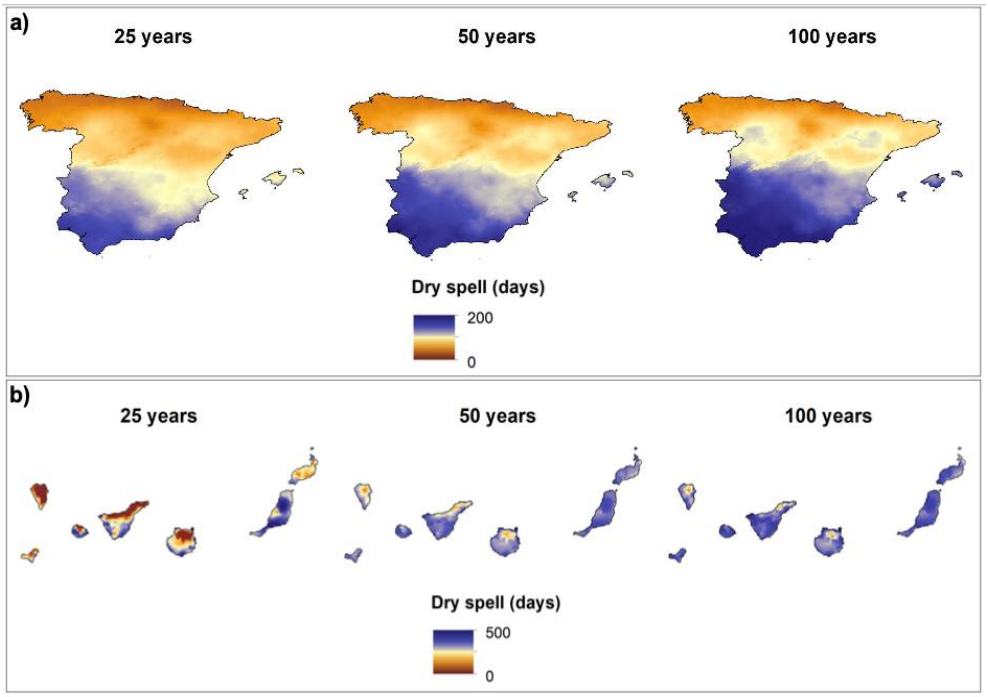

Figure 9. Quantile estimations for the dry spell length for periods of 25, 50 and 100 years in the Iberian Peninsula and Balearic Islands (**a**), and Canary islands (**b**).

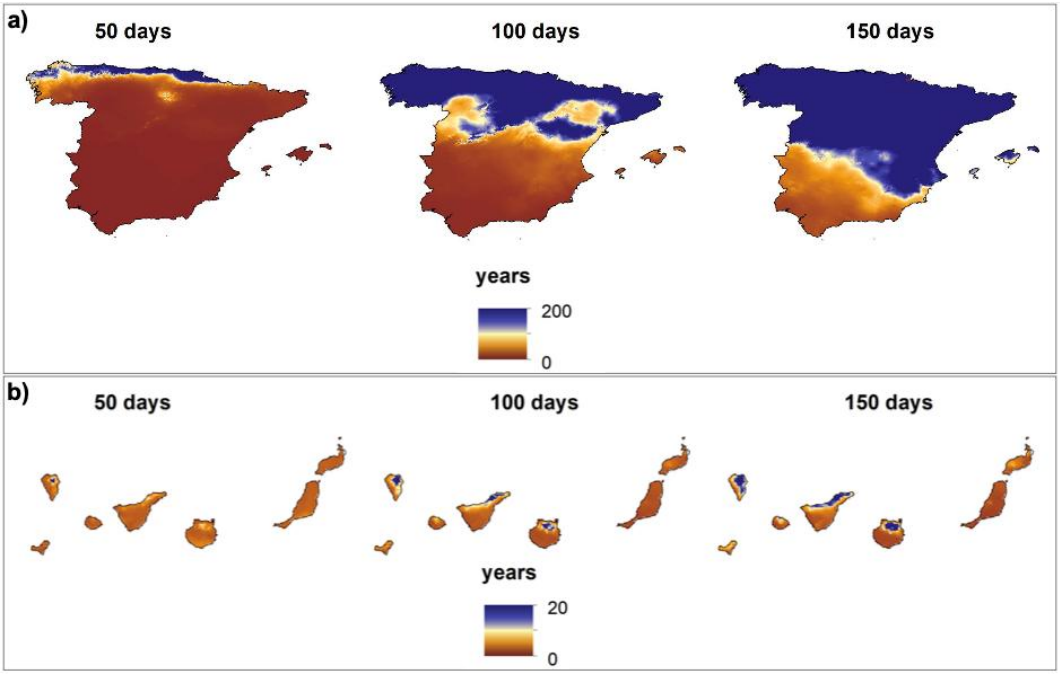

Figure 10. Return period in years corresponding to different magnitudes of precipitation and days of the dry spell length: Iberian Peninsula and Balearic Islands (**a**) and Canary Islands (**b**).

Finally, the agreement between station-based and interpolated estimates of the maximum dry-spell duration expected over 20 years (Figure 11) confirms the accuracy of the spatial interpolation. A near-linear relationship is observed in both mainland and island territories. Error statistics (Table 2) demonstrate a strong match between observed and predicted values (n = 2840 for mainland Spain and Balearic Islands; n = 72 for the Canary Islands), reinforcing the reliability of the hazard assessment maps.

These interpolated parameters were integrated into an interactive dry-spell hazard estimation tool "https://rachas-secas.csic.es/ (accessed on 29 September 2025)" which allows users to select custom dry-spell quantiles and return periods, and to visualize and download corresponding maps and point-specific curves.

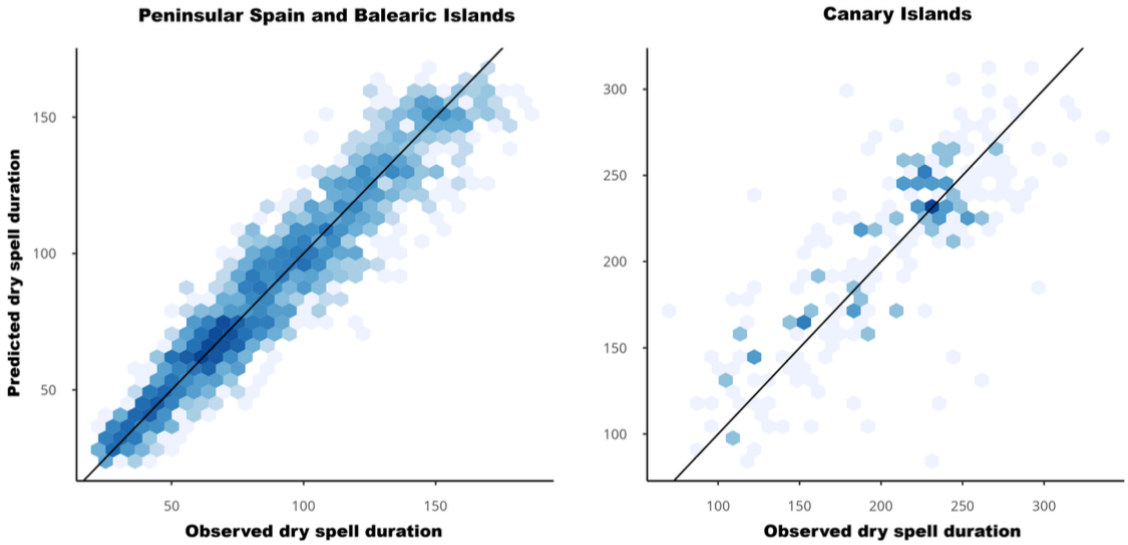

Figure 11. Cross-validation of the maximum dry-spell duration expected over the 20-year return period. The scatterplots compare values calculated from on-site GP distribution parameters (observed) with those estimated using interpolated parameters (predicted) for all stations. Colors represent point density, and the 1:1 line indicates perfect agreement.

Table 2. Cross-validation statistics for the predicted quantiles based on the interpolated parameters versus the observed quantiles at the station level corresponding to the maximum dry spell in 20 years. Metrics are computed using all paired observations from the cross-validation procedure. MAE = Mean Absolute Error; ME = Mean Error; rCD = coefficient of determination for cumulative distribution; r = Pearson correlation coefficient; KGE = Kling–Gupta Efficiency; D = Willmott's agreement index.

	MAE	ME	rCD	r	KGE	D
Peninsular Spain	7.77	−0.05	0.97	0.95	0.95	0.98
Canary Islands	26.6	2.73	0.97	0.77	0.77	0.88

4. Discussion

This study presents, for the first time, hazard probability maps for long dry spells across Spain. In fact, it is one of the few existing examples in the scientific literature that develops probabilistic maps for long-duration dry spells. While some previous efforts have mapped dry spell probabilities in specific regions—such as Ethiopia [64], parts of Spain [65], Greece [66], or at low spatial resolution in Europe [67], to our knowledge, no previous work has produced such high-resolution (2.5 km) maps with high accuracy and the added flexibility to estimate either dry spell quantiles for specific return periods or return periods for specified dry spell durations. This flexibility is made possible by the accurate spatial mapping of the parameters of the Generalized Pareto Distribution (GPD) across Spain. Although the approach of spatially interpolating distribution parameters has been used for the assessment of extreme precipitation events [33,34,61], this is the first application of such a methodology for dry spells in Spain.

Our results demonstrate the high accuracy of modeling dry spell durations exceeding the 90th percentile using the GP distribution. Compared to the traditional approach of using annual maximum values, this method provides a clear improvement in assessing dry spell hazard probabilities [46]. While other statistical distributions such as Weibull [67,68] or Wakeby [65] have been proposed, several studies have demonstrated the statistical robustness and suitability of the GPD for modeling dry spell hazard probabilities [35,46,55]. Our findings, based on a large network of meteorological stations spanning diverse climatic regions, reinforce this conclusion, with strong agreement observed between the empirical and GP-modeled cumulative distribution functions. It is important to note that the shape parameter κ showed lower validation performance compared to the other GP parameters, which is consistent with previous studies highlighting its higher uncertainty at local scales. This limitation arises because κ governs the tail behavior of the distribution and is therefore more sensitive to sampling variability and the limited number of extreme dry spells. For users of the data, this implies that caution is needed when interpreting return levels in areas with sparse station coverage, as uncertainty in κ can propagate to the estimation of very long return periods. Nevertheless, the spatial coherence observed in κ, particularly in the Canary Islands, and the strong agreement between observed and predicted return periods (Table 2) support the relevance of mapping this parameter rather than assuming a constant value.

Furthermore, this approach significantly outperforms alternatives such as Markov chains [69,70] or censored-data distributions, which fail to accurately represent the most extreme dry spells [25,71]—those that generate the most impactful socio-economic and environmental consequences, and which are the focus of this study.

The resulting maps surpass previous attempts to assess dry spell hazard in Spain. For instance, [25] proposed a regionalization of Spain based on dry spell statistics from a limited number of stations, using Markov chains, which tend to underestimate hazard probabilities across large areas. Similarly, [67] produced dry spell quantile maps for Europe with a general north-south gradient, a pattern also observed in our results. However, their coarse resolution did not allow for detailed spatial differentiation. The north-south gradient in dry spell probability is primarily driven by the varying influence of subtropical air masses during summer [72]. When these stable conditions extend into spring and autumn, very long dry spells can occur, with significant consequences for agriculture and water resources [6,41].

A major advancement of our work lies in the generation of spatially continuous parameter maps, which enable flexible estimation of dry spell quantiles. Thanks to the high quality of these interpolations, we demonstrate that calculating quantiles from interpolated parameters not only performs well for extreme precipitation—as highlighted by earlier studies [59,60]—but also yields high accuracy in estimating long-duration dry spells. Beyond generating static maps, we also developed an interactive climate service tool that allows users to query dry spell quantiles and return periods at both regional and site-specific scales. While recent advances in climate services have focused on indices, seasonal forecasts, or climate projections [73,74], to our knowledge, this product is the first tool dedicated specifically to user-defined dry spell quantiles and return periods. Additionally, it features a detailed graphical interface that enhances the usability and interpretation of both spatial and point-level outputs.

This science-based service has significant potential for agricultural, ecological, and environmental applications in Spain, where long dry spells are a major risk. Moreover, the flexible methodology is transferable to other regions worldwide—particularly in developing countries where dry spells cause major crop losses. With sufficient meteorological data, this framework can be implemented to generate accurate, user-oriented estimations of extreme dry spell quantiles and return periods, potentially improving agricultural planning and climate resilience.

A limitation of this study is the assumption of stationarity in the statistical properties of dry spell durations. It may not fully capture low-frequency internal climate variability or potential long-term shifts that are not represented within the observational period.

Another limitation is the relatively low accuracy in estimating the shape parameter (κ), as shown in Table 1. This parameter strongly influences the upper tail of the distribution, so its uncertainty mainly affects the estimation of very long return periods (e.g., >100 years), whereas estimates for moderate return periods remain robust. These limitations highlight the need for caution when interpreting results for extremely rare events and suggest that future work should explore non-stationary extreme value models, adaptive recalibration strategies as new data become available, and advanced approaches such as hierarchical or Bayesian methods to improve κ estimation in data-sparse regions.

5. Conclusions

This study delivers the first high-resolution (2.5 km) hazard probability maps for long-duration dry spells across Spain, addressing a critical gap in drought risk assessment. By applying extreme value theory and spatial interpolation of Generalized Pareto parameters, we provide a robust framework for estimating dry-spell quantiles and return periods across diverse climatic regions. Beyond the methodological contribution, a major achievement of this work is the development of an operational climate service through an interactive online platform "https://rachas-secas.csic.es/ (accessed on 29 September 2025)", which allows users to easily query site-specific hazard estimates and download data. This tool is designed to support decision-making in sectors such as water resource management, agriculture, and environmental planning, offering a user-friendly interface and transparent outputs. Together, these elements strengthen the capacity for drought risk management and provide a foundation for future updates and extensions of the service.

The main conclusions of this study are:

- Dry spell durations were effectively modeled using the Generalized Pareto Distribution, with parameters spatially interpolated using universal kriging, achieving strong agreement with empirical station data across 2840 stations.
- Parameter mapping and jackknife validation confirmed high model performance (e.g., KGE and agreement indices >0.9 for most parameters), even in climatically complex areas like the Canary Islands.
- The results reveal a consistent north-south gradient in dry spell severity, with the most prolonged and frequent dry spells occurring in southern and southeastern Spain and the arid eastern Canary Islands.
- This study delivers the first high-resolution (2.5 km) maps of dry spell hazard probabilities across Spain, significantly advancing climate services for drought risk management.
- As an outcome of this study, an interactive platform was developed, allowing users to explore and download dry spell hazard maps and return period data at fine spatial scales.
- The flexible, data-driven methodology is adaptable to other drought-prone regions worldwide, offering a valuable tool for climate adaptation planning in sectors like agriculture, water management, and conservation.

The interactive platform provides two main functionalities: (i) users can select a dry-spell duration (in days) to visualize the associated return period (in years) for each grid cell, or (ii) specify a return period to obtain the expected dry-spell length across Spain. This dual approach allows flexible queries while maintaining a simple interface, where only two input fields are required and each visualization includes clear legends for interpretation. When a user clicks on a specific location, a pop-up graph displays the magnitude–frequency curve, with the x-axis representing return periods (years) and the y-axis the corresponding dry-spell duration. The "Días" input box modifies the threshold for which the return period is calculated, while the "Años" axis in the pop-up reflects the full range of return periods for context. Unlike real-time monitoring services, this platform does not require continuous updates; recalibration will only be necessary when a substantial new volume of precipitation data becomes available. The full gridded dataset is also accessible for download through the platform, and a DOI is provided for citation and reproducibility. This tool complements existing climate services in Spain by focusing specifically on drought-related hazards and is intended for a wide range of users, including water resource managers, agricultural planners, and environmental agencies, supporting decision-making processes at both local and regional scales. An important limitation is that the methodology assumes stationary statistical properties of

dry spells observed. Users of the interactive tool should therefore interpret these results as representative of past and current climate conditions, not as projections. For long-term planning, these estimates should be complemented with climate model projections or non-stationary approaches to better account for possible future changes.

Author Contributions

A.H.-M.: conceptualization, visualization, writing—original draft preparation; S.B.: data curation, software, validation, writing—reviewing and editing; F.R.: data curation, software, validation, writing—reviewing and editing; A.R.-A.: data curation, investigation, software, validation, writing—reviewing and editing; M.A.: data curation, investigation, software, visualization, writing—reviewing and editing; M.G.-G.: data curation, software, validation, writing—reviewing and editing; B.L.: writing—reviewing and editing; A.E.K.: writing—reviewing and editing; M.F.: writing—reviewing and editing; M.A-M.: writing—reviewing and editing; A.C.: writing—reviewing and editing; D.P.-P.: writing—reviewing and editing; F.D.-C.: writing—reviewing and editing; J.M.G.: writing—reviewing and editing; C.A.-M.: writing—reviewing and editing; L.G.: writing—reviewing and editing; R.N.: writing—reviewing and editing; S.M.V.-S.: conceptualization, methodology, visualization, writing—original draft preparation, validation, supervision. All authors have read and agreed to the published version of the manuscript.

Funding

This work has been supported by the research projects TED2021-129152B-C41 and PID2022-137244OB-I00, financed by the Spanish Ministry of Science and FEDER, CSIC's Interdisciplinary Thematic Platform Clima (PTI-Clima), contract CSC2023-02-00 financed by the Ministry for the Ecological Transition and the Demographic Challenge (MITECO) and the European Commission NextGenerationEU (Regulation EU 2020/2094) and GLANCE (ESA Contract No. 4000145543/24/I-LR).

Data Availability Statement

An interactive online platform "https://rachas-secas.csic.es/ (accessed on 29 September 2025)", allows users to easily query site-specific hazard estimates and download data. The data that support the findings of this study are available from the corresponding author upon reasonable request.

Acknowledgments

M.F. has been supported by the Grant JDC2022-048710-I funded by MCIN/AEI/https://doi.org/10.13039/501100011033 and by the European Union NextGenerationEU/PRTR. The Climatoc-Lab was also supported by the RED-CLIMA 2 project funded by CSIC (Ref. LINCG24042) and the PROMETEO Grant CIPROM/2023/38 for Excellence Research Groups funded by the GVA. EPhysLab members were supported by the following projects TED2021-129152B-C43, funded by the Ministerio de Ciencia, Innovación y Universidades, Spain, and Xunta de Galicia (ED431C2021/44; Programa de Consolidación e Estructuración de Unidades de Investigación Competitivas (Grupos de Referencia Competitiva), Consellería de Cultura, Educación e Universidade) funded by the European Commission 'ERDF A way of making Europe' program and "NextGenerationEU"/PRTR. EPhysLab computing has also been possible thanks to the computing resources and technical support provided by CESGA (Centro de Supercomputación de Galicia) and RES (Red Española de Supercomputación). Also, the authors would like to thank the Spanish Meteorological Agency (AEMET) for granting access to the National Climate Data Bank, which made this study possible.

Conflicts of Interest

Given the role as Editor-in-Chief, S. M. Vicente-Serrano had no involvement in the peer review of this paper and had no access to information regarding its peer-review process. Full responsibility for the editorial process of this paper was delegated to another editor of the journal.

References

1. Vicente-Serrano, S.M.; Quiring, S.M.; Peña-Gallardo, M.; et al. A review of environmental droughts: Increased risk under global warming? *Earth-Sci. Rev.* **2020**, *201*, 102953. https://doi.org/10.1016/j.earscirev.2019.102953.
2. Vogt, J.; Erian, W.; Pulwarty, R.; et al. *GAR Special Report on Drought 2021 (United Nations)*; United Nations Office for Disaster Risk Reduction: Geneva, Switzerland, 2021.

3. AghaKouchak, A.A baseline probabilistic drought forecasting framework using standardized soil moisture index: Application to the 2012 United States drought. *Hydrol. Earth Syst. Sci.* **2014**, *18*, 2485–2492. https://doi.org/10.5194/hess-18-2485-2014.
4. Padrón, R.S.; Gudmundsson, L.; Decharme, B.; et al. Observed changes in dry-season water availability attributed to human-induced climate change. *Nat. Geosci.* **2020**, *13*, 477–481. https://doi.org/10.1038/s41561-020-0594-1.
5. Barker, L.J.; Hannaford, J.; Parry, S.; et al. Historic hydrological droughts 1891–2015: Systematic characterisation for a diverse set of catchments across the UK. *Hydrol. Earth Syst. Sci.* **2019**, *23*, 4583–4602. https://doi.org/10.5194/hess-23-4583-2019.
6. Lorenzo-Lacruz, J.; Vicente-Serrano, S.M.; González-Hidalgo, J.C.; et al. Hydrological drought response to meteorological drought in the Iberian Peninsula. *Clim. Res.* **2013**, *58*, 117–131. https://doi.org/10.3354/cr01177.
7. Heim, R.R. A Review of Twentieth-Century Drought Indices Used in the United States. *Bull. Am. Meteorol. Soc.* **2002**, *83*, 1149–1165. https://doi.org/10.1175/1520-0477(2002)083<1149:AROTDI>2.3.CO;2.
8. Palmer, W.C.; Meteorological drought. *Weather Bureau Res. Paper* **1965**, *45*, 1–58.
9. Vicente-Serrano, S.M.; Beguería, S.; López-Moreno, J.I. A multiscalar drought index sensitive to global warming: The standardized precipitation evapotranspiration index. *J. Clim.* **2010**, *23*, 1696–1718. https://doi.org/10.1175/2009JCLI2909.1.
10. Vicente-Serrano, S.M.; Domínguez-Castro, F.; Beguería, S.; et al. Atmospheric drought indices in future projections. *Nat. Water* **2025**, *3*, 374–387. https://doi.org/10.1038/s44221-025-00416-9.
11. Domínguez-Castro, F.; Vicente-Serrano, S.M.; Tomás-Burguera, M.; et al. High-spatial-resolution probability maps of drought duration and magnitude across Spain. *Nat. Hazards Earth Syst. Sci.* **2019**, *19*, 611–628. https://doi.org/10.5194/nhess-19-611-2019.
12. González, J.; Valdés, J.B. The mean frequency of recurrence of in-time-multidimensional events for drought analyses. *Nat. Hazards Earth Syst. Sci.* **2004**, *4*, 17–28. https://doi.org/10.5194/nhess-4-17-2004.
13. Onyutha, C. On Rigorous Drought Assessment Using Daily Time Scale: Non-Stationary Frequency Analyses, Revisited Concepts, and a New Method to Yield Non-Parametric Indices. *Hydrology* 2017, 4. https://doi.org/10.3390/hydrology4040048.
14. Vicente-Serrano, S.M.; Peña-Angulo, D.; Beguería, S.; et al. Global drought trends and future projections. *Philos. Trans. R. Soc. A Math. Phys. Eng. Sci.* **2022**, *380*, 20210285. https://doi.org/10.1098/rsta.2021.0285.
15. Anderegg, W.R.L.; Kane, J.M.; Anderegg, L.D.L. Consequences of widespread tree mortality triggered by drought and temperature stress. *Nat. Clim. Chang.* **2013**, *3*, 30–36. https://doi.org/10.1038/nclimate1635.
16. Kim, W.; Iizumi, T.; Nishimori, M. Global Patterns of Crop Production Losses Associated with Droughts from 1983 to 2009. *J. Appl. Meteorol. Climatol.* **2019**, *58*, 1233–1244. https://doi.org/10.1175/JAMC-D-18-0174.1.
17. Gincheva, A.; Pausas, J.G.; Torres-Vázquez, M.Á.; et al. The Interannual Variability of Global Burned Area Is Mostly Explained by Climatic Drivers. *Earth's Future* **2024**, *12*, e2023EF004334. https://doi.org/10.1029/2023EF004334.
18. Iglesias, E.; Garrido, A.; Gómez-Ramos, A. Evaluation of drought management in irrigated areas. *Agric. Econ.* **2003**, *29*, 211–229. https://doi.org/10.1016/S0169-5150(03)00084-7.
19. Lopez-Nicolas, A.; Pulido-Velazquez, M.; Macian-Sorribes, H. Economic risk assessment of drought impacts on irrigated agriculture. *J. Hydrol.* **2017**, *550*, 580–589. https://doi.org/10.1016/J.JHYDROL.2017.05.004.
20. Martínez-Ibarra, E. Climate, water and tourism: Causes and effects of droughts associated with urban development and tourism in Benidorm (Spain). *Int. J. Biometeorol.* **2015**, *59*, 487–501. https://doi.org/10.1007/s00484-014-0851-3.
21. Christian, J.I.; Basara, J.B.; Hunt, E.D.; et al. Flash drought development and cascading impacts associated with the 2010 Russian heatwave. *Environ. Res. Lett.* **2020**, *15*, 094078. https://doi.org/10.1088/1748-9326/AB9FAF.
22. Caloiero, T.; Coscarelli, R. Analysis of the Characteristics of Dry and Wet Spells in a Mediterranean Region. *Environ. Process.* **2020**, *7*, 691–701. https://doi.org/10.1007/s40710-020-00454-3.
23. el Hafyani, M.; Khalid, E. Literature Review on Stochastic Modeling of Wet and Dry Spells. *J. Environ. Earth Sci.* **2024**, *6*, 241–260. https://doi.org/10.30564/jees.v6i3.6964.
24. Ferijal, T.; Mechram, S.; Fauzi, A. Spatial and temporal analysis of dry spell variability in Aceh, Indonesia: Implications for drought mitigation and agricultural planning. *IOP Conf. Ser. Earth Environ. Sci.* **2025**, *1476*, 012009. https://doi.org/10.1088/1755-1315/1476/1/012009.
25. Martin-Vide, J.; Gomez, L. Regionalization of Peninsular Spain based on the length of dry spells. *Int. J. Climatol.* **1999**, *19*, 537–555. https://doi.org/10.1002/(SICI)1097-0088(199904)19:5<537::AID-JOC371>3.0.CO;2-X.
26. Sirangelo, B.; Caloiero, T.; Coscarelli, R.; et al. A Stochastic Approach for the Analysis of Long Dry Spells with Different Threshold Values in Southern Italy. *Water* **2019**, *11*, 2026. https://doi.org/10.3390/w11102026.
27. Breinl, K.; Di Baldassarre, G.; Mazzoleni, M.; et al. Extreme dry and wet spells face changes in their duration and timing. *Environ. Res. Lett.* **2020**, *15*, 074040. https://doi.org/10.1088/1748-9326/ab7d05.
28. Manning, C.; Widmann, M.; Bevacqua, E.; et al. Increased probability of compound long-duration dry and hot events in Europe during summer (1950–2013). *Environ. Res. Lett.* **2019**, *14*, 094006. https://doi.org/10.1088/1748-9326/ab23bf.

29. Raymond, F.; Drobinski, P.; Ullmann, A.; et al. Extreme dry spells over the Mediterranean Basin during the wet season: Assessment of HyMeX/Med-CORDEX regional climate simulations (1979–2009). *Int. J. Climatol.* **2018**, *38*, 3090–3105. https://doi.org/10.1002/joc.5487.
30. Rivoire, P.; Tramblay, Y.; Neppel, L.; et al. Impact of the dry-day definition on Mediterranean extreme dry-spell analysis. *Nat. Hazards Earth Syst. Sci.* **2019**, *19*, 1629–1638. https://doi.org/10.5194/nhess-19-1629-2019.
31. Beguería, S.; Vicente-Serrano, S.M.; López-Moreno, J.I.; et al. Annual and seasonal mapping of peak intensity, magnitude and duration of extreme precipitation events across a climatic gradient, northeast Spain. *Int. J. Climatol.* **2009**, *29*, 1759–1779. https://doi.org/10.1002/joc.1808.
32. Catalini, C.G.; Guillen, N.F.; Bazzano, F.M.; et al. Web Mapping of Extreme Daily Rainfall Data in Central and Northern Argentina. *J. Hydrol. Eng.* **2021**, *26*, 05021013. https://doi.org/10.1061/(ASCE)HE.1943-5584.0002077.
33. Formetta, G.; Dallan, E.; Borga, M.; et al. Sub-daily precipitation returns levels in ungauged locations: Added value of combining observations with convection permitting simulations. *Adv. Water Resour.* **2024**, *194*, 104851. https://doi.org/10.1016/j.advwatres.2024.104851.
34. Iliopoulou, T.; Koutsoyiannis, D.; Malamos, N.; et al. A stochastic framework for rainfall intensity–time scale–return period relationships. Part II: Point modelling and regionalization over Greece. *Hydrol. Sci. J.* **2024**, *69*, 1092–1112. https://doi.org/10.1080/02626667.2024.2345814.
35. Cindrić Kalin, K.; Pasarić, Z. Regional patterns of dry spell durations in Croatia. *Int. J. Climatol.* **2022**, *42*, 5503–5519. https://doi.org/10.1002/joc.7545.
36. Sarhadi, A.; Heydarizadeh, M. Regional frequency analysis and spatial pattern characterization of Dry Spells in Iran. *Int. J. Climatol.* **2014**, *34*, 835–848. https://doi.org/10.1002/joc.3726.
37. González-Hidalgo, J.C.; Vicente-Serrano, S.M.; Peña-Angulo, D.; et al. High-resolution spatio-temporal analyses of drought episodes in the western Mediterranean basin (Spanish mainland, Iberian Peninsula). *Acta Geophys.* **2018**, *66*, 381–392. https://doi.org/10.1007/s11600-018-0138-x.
38. Trullenque-Blanco, V.; Beguería, S.; Vicente-Serrano, S.M.; et al. Catalogue of drought events in peninsular Spanish along 1916–2020 period. *Sci. Data* **2024**, *11*, 703. https://doi.org/10.1038/s41597-024-03484-w.
39. Camarero, J.J.; Gazol, A.; Sangüesa-Barreda, G.; et al. Forest growth responses to drought at short- and long-term scales in Spain: Squeezing the stress memory from tree rings. *Front. Ecol. Evol.* **2018**, *6*, 9. https://doi.org/10.3389/fevo.2018.00009.
40. Iglesias, A.; Rosenzweig, C.; Pereira, D. Agricultural impacts of climate change in Spain: Developing tools for a spatial analysis. *Glob. Environ. Chang.* **2000**, *10*, 69–80. https://doi.org/10.1016/S0959-3780(00)00010-8.
41. Peña-Gallardo, M.; Martín Vicente-Serrano, S.; Domínguez-Castro, F.; et al. The impact of drought on the productivity of two rainfed crops in Spain. *Nat. Hazards Earth Syst. Sci.* **2019**, *19*, 1215–1234. https://doi.org/10.5194/nhess-19-1215-2019.
42. Vicente-Serrano, S.M.; Peña-Angulo, D.; Murphy, C.; et al. The complex multi-sectoral impacts of drought: Evidence from a mountainous basin in the Central Spanish Pyrenees. *Sci. Total Environ.* **2021**, *769*, 144702. https://doi.org/10.1016/j.scitotenv.2020.144702.
43. Vicente-Serrano, S.M.; Beguería, S.; López-Moreno, J.I.; et al. A complete daily precipitation database for northeast Spain: Reconstruction, quality control, and homogeneity. *Int. J. Climatol.* **2010**, *30*, 1146–1163. https://doi.org/10.1002/joc.1850.
44. Beguería, S.; Tomas-Burguera, M.; Serrano-Notivoli, R.; et al. Gap filling of monthly temperature data and its effect on climatic variability and trends. *J. Clim.* **2019**, *32*, 7797–7821. https://doi.org/10.1175/JCLI-D-19-0244.1.
45. Beguería, S.; Tomas-Burguera, M.; Serrano-Notivoli, R.; et al. Evolution of extreme precipitation in Spain: Contribution of atmospheric dynamics and long-term trends. *Stoch. Environ. Res. Risk Assess.* **2025**, *39*, 2137–2157. https://doi.org/10.1007/s00477-025-02961-x.
46. Vicente-Serrano, S.M.; Beguería-Portugués, S. Estimating extreme dry-spell risk in the middle Ebro valley (northeastern Spain): A comparative analysis of partial duration series with a general Pareto distribution and annual maxima series with a Gumbel distribution. *Int. J. Climatol.* **2003**, *23*, 1103–1118. https://doi.org/10.1002/joc.934.
47. Lana, X.; Burgueño, A. Probabilities of Repeated Long Dry Episodes Based on the Poisson Distribution. An example for Catalonia (NE Spain). *Theor. Appl. Climatol.* **1998**, *60*, 111–120. https://doi.org/10.1007/s007040050037.
48. Davy, L. Une nouvelle approache de la Sécheresse dans le basin de l'Ebre étude des épisodes secs. *Revue Géographique de l'Est* **1975**, **1–2**, 153–167.
49. Racsko, P.; Szeidl, L.; Semenov, M. A serial approach to local stochastic weather models. *Ecol. Model.* **1991**, *57*, 27–41. https://doi.org/10.1016/0304-3800(91)90053-4.
50. Douguedroit, A. The variations of dry spells in marseilles from 1865 to 1984. Journal of Climatology **1987**, *7*, 541–551. https://doi.org/10.1002/joc.3370070603.
51. Nobilis, F. Dry spells in the Alpine country Austria. *J. Hydrol.* **1986**, *88*, 235–251. https://doi.org/10.1016/0022-1694(86)90093-4.
52. Hershfield, D.M. on the probability of extreme rainfall events. *Bull. Am. Meteorol. Soc.* **1973**, *54*, 1013–1018. https://doi.org/10.1175/1520-0477(1973)054<1013:OTPOER>2.0.CO;2.

53. Caeiro, F.; Gomes, M. *Threshold Selection in Extreme Value Analysis*; Chapman and Hall/CRC: Boca Raton, FL, USA, 2014.
54. Pickands, J., III. Statistical Inference Using Extreme Order Statistics. *Ann. Stat.* **1975**, *3*, 119–131. https://doi.org/10.1214/aos/1176343003.
55. She, D.; Xia, J.; Song, J.; et al. Spatio-temporal variation and statistical characteristic of extreme dry spell in Yellow River Basin, China. *Theor. Appl. Climatol.* **2013**, *112*, 201–213. https://doi.org/10.1007/s00704-012-0731-x.
56. Hosking, J.R.M.; Wallis, J.R. Parameter and Quantile Estimation for the Generalized Pareto Distribution. *Technometrics* **1987**, *29*, 339–349. https://doi.org/10.1080/00401706.1987.10488243.
57. Miniussi, A.; Marra, F. Estimation of extreme daily precipitation return levels at-site and in ungauged locations using the simplified MEV approach. *J. Hydrol.* **2021**, *603*, 126946. https://doi.org/10.1016/j.jhydrol.2021.126946.
58. Zou, W.; Yin, S.; Wang, W. Spatial interpolation of the extreme hourly precipitation at different return levels in the Haihe River basin. *J. Hydrol.* **2021**, *598*, 126273. https://doi.org/10.1016/j.jhydrol.2021.126273.
59. Das, S.; Zhu, D.; Yin, Y. Comparison of mapping approaches for estimating extreme precipitation of any return period at ungauged locations. *Stoch. Environ. Res. Risk Assess.* **2020**, *34*, 1175–1196. https://doi.org/10.1007/s00477-020-01828-7.
60. Yin, S.; Wang, Z.; Zhu, Z.; et al. Using Kriging with a heterogeneous measurement error to improve the accuracy of extreme precipitation return level estimation. *J. Hydrol.* **2018**, *562*, 518–529. https://doi.org/10.1016/j.jhydrol.2018.04.064.
61. Beguería, S.; Vicente-Serrano, S.M. Mapping the hazard of extreme rainfall by peaks over threshold extreme value analysis and spatial regression techniques. *J. Appl. Meteorol. Climatol.* **2006**, *45*, 108–124. https://doi.org/10.1175/JAM2324.1.
62. Burrough, P.A.; McDonnell, R.A. Principle of Geographic Information Systems. *Oxford University Press*: New York, NY, USA, 1998. Available online: https://www.researchgate.net/publication/37419765 (accessed on 29 September 2025).
63. Willmott, C.J.; Robeson, S.M.; Matsuura, K. A refined index of model performance. *Int. J. Climatol.* **2012**, *32*, 2088–2094. https://doi.org/10.1002/joc.2419.
64. Tegegn, M.G.; Berlie, A.B.; Utallo, A.U. Patterns and probabilities of dry spells and rainfall for improved rain-fed farming in Northwestern Ethiopia. *Discov. Sustain.* **2024**, *5*, 387. https://doi.org/10.1007/s43621-024-00576-w.
65. Pérez-Sánchez, J.; Senent-Aparicio, J. Analysis of meteorological droughts and dry spells in semiarid regions: A comparative analysis of probability distribution functions in the Segura Basin (SE Spain). *Theor. Appl. Climatol.* **2018**, *133*, 1061–1074. https://doi.org/10.1007/s00704-017-2239-x.
66. Anagnostopoulou, C.; Maheras, P.; Karacostas, T.; et al. Spatial and temporal analysis of dry spells in Greece. *Theor. Appl. Climatol.* **2003**, *74*, 77–91. https://doi.org/10.1007/s00704-002-0713-5.
67. Serra, C.; Martínez, M.D.; Lana, X.; et al. European dry spell length distributions, years 1951–2000. *Theor. Appl. Climatol.* **2013**, *114*, 531–551. https://doi.org/10.1007/s00704-013-0857-5.
68. Vargas, W.M.; Naumann, G.; Minetti, J.L. Dry spells in the River Plata Basin: An approximation of the diagnosis of droughts using daily data. *Theor. Appl. Climatol.* **2011**, *104*, 159–173. https://doi.org/10.1007/s00704-010-0335-2.
69. Avilés, A.; Célleri, R.; Solera, A.; et al. Probabilistic Forecasting of Drought Events Using Markov Chain- and Bayesian Network-Based Models: A Case Study of an Andean Regulated River Basin. *Water* **2016**, *8*, 37. https://doi.org/10.3390/w8020037.
70. López-Franca, N.; Sánchez, E.; Losada, T.; et al. Markovian characteristics of dry spells over the Iberian Peninsula under present and future conditions using ESCENA ensemble of regional climate models. *Clim. Dyn.* **2015**, *45*, 661–677. https://doi.org/10.1007/s00382-014-2280-8.
71. Perzyna, G. Spatial and temporal characteristics of maximum dry spells in Southern Norway. *Int. J. Climatol.* **1994**, *14*, 895–909. https://doi.org/10.1002/joc.3370140806.
72. Martin-Vide, J.; Olcina-Cantos, J. *Climas y tiempos de España*, *Alianza Editorial*; Alianza: Madrid, Spain, 2001; p. 43.
73. Hempelmann, N.; Ehbrecht, C.; Alvarez-Castro, C.; et al. Web processing service for climate impact and extreme weather event analyses. Flyingpigeon (Version 1.0). *Comput. Geosci.* **2018**, *110*, 65–72. https://doi.org/10.1016/j.cageo.2017.10.004.
74. Street, R.B. Towards a leading role on climate services in Europe: A research and innovation roadmap. *Clim. Serv.* **2016**, *1*, 2–5. https://doi.org/10.1016/j.cliser.2015.12.001.